Physica B 407 (2012) 689–693

Contents lists available at SciVerse ScienceDirect

Physica B

journal homepage: www.elsevier.com/locate/physb

Temperature-dependent features of $Pb_3Mn_7O_{15}$ crystal structure

N.V. Volkov [a,b], L.A. Solovyov [c], E.V. Eremin [a], K.A. Sablina [a], S.V. Misjul [b], M.S. Molokeev [a], A.I. Zaitsev [a], M.V. Gorev [a], A.F. Bovina [a], N.V. Mihashenok [a,*]

[a] L.V. Kirensky Institute of Physics, SB RAS, Krasnoyarsk 660036, Russia
[b] Institute of Engineering Physic and Radioelectronic of Siberian State University, Krasnoyarsk 630074, Russia
[c] Institute of Chemistry and Chemical Technology, SB RAS, Krasnoyarsk 660049, Russia

ARTICLE INFO

Article history:
Received 13 September 2011
Received in revised form
28 November 2011
Accepted 28 November 2011
Available online 13 December 2011

Keywords:
Manganese
Layered compounds
X-ray diffraction

ABSTRACT

The results of X-ray diffraction (XRD) structural investigations of $Pb_3Mn_7O_{15}$ crystals carried out for a wide temperature range including the room temperature are presented. It has been observed for the first time that with increasing temperature the $Pb_3Mn_7O_{15}$ crystals transform from the orthorhombic (Pnma space group) to the hexagonal ($P6_3/mcm$ space group) structure. The results of the thermal analysis have revealed two sharp peaks in the temperature dependence correlating with the XRD data. According to the results of the group-theoretical analysis, the $Pb_3Mn_7O_{15}$ symmetry transformation can be described as $P6_3/mcm \xrightarrow[(\eta,0,0)]{M_2^+(12-4)}$ Pnma.

1. Introduction

Having reviewed the existing works devoted to the structure of $Pb_3Mn_7O_{15}$, we faced with contradictory data reported. In particular, Darriet et al. [1] described the structure of $Pb_3Mn_7O_{15}$ as orthorhombic noncentrosymmetrical with the Cmc2 space group. Then, March et al. [2] defined the symmetry of this material as centrosymmetrical Cmcm. Later, the structure was refined by Le Page et al. [3] who showed that using the hexagonal $P6_3/mcm$ space group considerably improved the structural parameters. The $P6_3/mcm$ symmetry was confirmed in [4] on both powder and single-crystal samples by XRD studies. The authors investigated the native mineral Zenzenite with the general formula $Pb_3(Fe^{3+}Mn^{3+})_4Mn_3^{4+}O_{15}$ indexed in the hexagonal structure. In the mentioned studies, all the measurements were performed at room temperature.

Our interest to $Pb_3Mn_7O_{15}$ as a compound containing manganese ions of different valence is caused by the following. The well-known perovskite-like manganites, which still have been intensively studied, allow variation of the ratio between the manganese ions with different valence by substitution, thus changing fundamentally the magnetic and electrical properties of the materials. These compounds are characterized by such interesting properties as charge and orbital ordering, metal-dielectric transition, colossal magnetoresistance, coexistence of the magnetic phases with competing ferro- and antiferromagnetic interactions, magnetic phase stratification, etc. A structural feature of the perovskite-like manganites is the presence of layers that contain manganese ions located in oxygen octahedral vertex connected, which is one of the grounds for the formation of a rich variety of the mentioned properties.

Some recent studies deal with the manganese-bearing compounds where manganese layers contain manganese ions of different valence, like in perovskites, but the oxygen octahedra are connected at their edge-sharing, as in $Pb_3Mn_5V_2O_{16}$ [5], $BaMn_3O_6$ [6], etc [7–9]. The material of our interest, $Pb_3Mn_7O_{15}$, belongs to such compounds. The lead-bearing compounds are also of interest since stereoactive Pb^{2+} ions with a $6s^2$ lone pair may provide the conditions for the occurrence of local dipoles in the system and, consequently, the formation of ferroelectric and antiferroelectric states [10]. The presence of the transition metal ions Mn in $Pb_3Mn_7O_{15}$ as a source of possible magnetic interactions and magnetic ordering and the local structural distortions can cause coupling between electric polarization and magnetism.

In the previous works [11–13], we reported the magnetic, dielectric, and calorimetric properties of the $Pb_3Mn_7O_{15}$ single crystals grown by spontaneous crystallization from solution in melt. We discovered anomalies in the temperature dependence of magnetization at $T_1=160$ K, $T_2=70$ K, and $T_3=20$ K [11], which were in good agreement with anomalies in the temperature dependence of specific heat [12]. The temperature dependences of ε' and ε'' revealed the sharp peaks strongly dependent on frequency and lying within 150–210 K [13]. The data obtained were interpreted basing on the hexagonal $P6_3/mcm$ space group with the lattice parameters $a=10.0287(4)$ Å and $c=13.6137(6)$ Å at room temperature.

Despite the extensive investigations, many unclear points have still remained, including the problem of the effect of structural

* Corresponding author. Tel.: +7 391 290 71 08; fax: +7 391 243 89 23.
E-mail address: stasha-83@yandex.ru (N.V. Mihashenok).

0921-4526/$ - see front matter © 2011 Elsevier B.V. All rights reserved.
doi:10.1016/j.physb.2011.11.058

distortions on the magnetic and other properties of $Pb_3Mn_7O_{15}$. The exact structure of this compound and the origin of local distortions have to be established.

The results of recent structural studies of our samples by the high-resolution synchrotron XRD technique in the temperature range 15–295 K were reported in [14]. The obtained structure is unambiguously orthorhombic with the Pnma space group over the entire temperature range. Using thermogravimetry (TG), we established that the oxygen content in the samples slightly differed from the stoichiometric $Pb_3Mn_7O_{15}$ composition and equals to 14.93 ± 0.05 [14].

In this study, we present XRD structural investigations of the $Pb_3Mn_7O_{15}$ crystals in a wide temperature range below and above room temperature. For the first time, we report the temperature dependences of the thermal expansion coefficient and the differential scanning calorimetry (DSC) data. To describe the structural transformations leading to the phase transition at high temperatures, we applied the group-theoretical methods and showed that the symmetry transformation in the $Pb_3Mn_7O_{15}$ crystals corresponds to the scheme $P6_3/mcm \xrightarrow[(\eta,0,0)]{M_2^-(12-4)} Pnma$.

2. Experimental details

Single crystals were grown by the flux method. As a flux, PbO was chosen, known as an effective solvent for many oxide compounds allowing to avoid incorporation of foreign ions into the lattice. Synthesis of the $Pb_3Mn_7O_{15}$ crystals started with heating of a mixture of appropriate amounts of high-purity PbO and Mn_2O_3 in a platinum crucible at 1000 °C for 4 h. Then, the crucible was slowly cooled to 900° with a rate of 2–5°/h; afterwards, the furnace was cooled to room temperature. The single crystals of a plate-hexagonal form with black shiny surfaces were found at a level of a solidified liquid surface. The plates were up to 40 mm in diameter. The grown crystals were extracted from the flux mechanically.

Single crystal X-ray diffraction data on $Pb_3Mn_7O_{15}$ were collected using diffractometer SMART APEX II (Bruker) with CCD detector. However interpretation of these data was very complicated because of several twin components in crystal. So we decided to solve structure from powder diffraction data. Powder X-ray diffraction (PXRD) data on $Pb_3Mn_7O_{15}$ were collected using a PANalytical X'Pert PRO diffractometer equipped with a PIXcel solid state detector and a secondary graphite monochromator (Cu Kα radiation). High-temperature measurements were performed using an Anton Paar HTK1200 camera with sample rotation and automated alignment. The full-profile analysis of the crystal structure was carried out applying the Rietveld formalism [15] and the derivative difference minimization (DDM) refinement method [16]. The measurements were performed within the temperature range 298–1100 K.

Low-temperature XRD data for a single-crystal plate were collected on a DRON-2 diffractometer (Cu Kα radiation).

The synchronous thermal analysis of the $Pb_3Mn_7O_{15}$ samples was performed with a STA 449C Jupiter TG/DSC device (NETZCH). A sample with a mass of 36.583 mg was placed in a standard platinum DSC crucible 6.8 mm in diameter and 5 mm height with a cover. Flow (35 ml/min) atmosphere consisting of 80% of pure argon and 20% of oxygen was used. The sample was heated to 1073 K and cooled to room temperature with a rate of 10 K/min.

The coefficient of thermal expansion was measured with a DIL-402C dilatometer (NETZSCH) in the temperature range 140–750 K in a dynamic mode with a heating rate of 3 K/min. Fused-quartz etalons were used for calibration and account for expansion of the measuring system. The plate sample with a thickness of 0.81 mm was measured along and across the plate.

3. Results

The crystal structure model of $Pb_3Mn_7O_{15}$ at 298 K was taken from Ref. [14] and confirmed by the refinement. The crystallographic data are summarized in Tables 1–4. The observed and calculated PXRD patterns after the crystal structure refinement are shown in Fig. 1a. According to the results of the high-temperature measurements, above 408 K the orthorhombic (pseudohexagonal) lattice of $Pb_3Mn_7O_{15}$ was transformed to an intermediate hexagonal lattice analogous to that of Zenzenite $Pb_3(Fe,Mn)_4Mn_3O_{15}$ [4]. Almost all the observed reflections were consistent with the hexagonal symmetry, except for some small peaks that could not be definitely assigned. Observed extra-peaks may correspond to an incommensurate modulation, which will be a matter of further research. The intermediate modulated structure was reversibly stabilized at heating/cooling between 391 and 562 K in agreement with the observed effects on the DSC curves (Fig. 2). Above 562 K, the additional peaks disappeared and the PXRD pattern was fully consistent with the hexagonal $P6_3/mcm$ symmetry. The high-temperature crystal structure of

Table 1
Crystal data for $Pb_3Mn_7O_{15}$.

Temperature (K)	298	573	1073
Crystal system	Orthorhombic	Hexagonal	Hexagonal
Space group	Pnma	$P6_3/mcm$	$P6_3/mcm$
Z	8	4	4
Cell parameters			
a (Å)	13.5939(1)	10.0337(1)	10.0939(1)
b (Å)	17.3027(5)	10.0337(1)	10.0939(1)
c (Å)	10.0305(1)	13.6288(2)	13.6896(1)
Volume (Å^3)	2359.28(7)	1188.25(2)	1207.93(2)
R-DDM (%)	7.39	9.26	6.95
R_{Bragg} (%)	2.83	2.96	2.31

Table 2
Atomic coordinates and isotropic displacement parameters for $Pb_3Mn_7O_{15}$ at 298 K.

Atom	Site	*x*	*y*	*z*	U_{iso} (Å^2)
Pb_{11}	4c	0.2415(2)	1/4	0.8559(2)	0.026(1)
Pb_{12}	8d	0.2508(1)	0.0561(1)	0.4399(2)	0.023(1)
Pb_{21}	4c	0.2294(1)	1/4	0.5099(2)	0.026(1)
Pb_{22}	8d	0.2426(1)	0.11865(8)	0.1114(1)	0.023(1)
Mn_{11}	8d	−0.0022(5)	0.0818(3)	0.257(1)	0.022(1)
Mn_{12}	8d	0.4901(4)	0.3355(4)	0.9906(8)	0.019(2)
Mn_{13}	8d	−0.0090(3)	0.1659(4)	0.0021(8)	0.017(2)
Mn_{21}	8d	0.6420(3)	0.4159(4)	0.7517(7)	0.012(2)
Mn_{22}	8d	0.8488(3)	0.0831(4)	0.7585(8)	0.012(2)
Mn_{31}	4c	−0.0129(6)	1/4	0.759(1)	0.012(2)
Mn_{32}	4a	0	0	0	0.017(2)
Mn_{33}	4b	0	0	1/2	0.018(2)
Mn_{41}	4c	−0.0086(6)	1/4	0.254(1)	0.016(2)
O_{11}	8d	0.582(1)	0.508(1)	0.686(3)	0.026(2)
O_{12}	8d	0.916(1)	0.993(1)	0.645(2)	0.026(2)
O_{13}	8d	0.579(2)	0.414(1)	0.910(2)	0.026(2)
O_{14}	8d	0.918(2)	0.084(1)	0.923(3)	0.026(2)
O_{15}	8d	0.564(2)	0.325(1)	0.656(2)	0.026(2)
O_{16}	8d	0.907(1)	0.166(1)	0.674(2)	0.026(2)
O_{21}	8d	0.257(1)	0.013(1)	0.657(2)	0.011(2)
O_{22}	8d	0.232(1)	0.160(1)	0.682(2)	0.011(2)
O_{23}	8d	0.253(2)	0.072(1)	0.892(2)	0.011(2)
O_{31}	4c	0.076(2)	1/4	0.110(3)	0.043(3)
O_{32}	4c	0.408(2)	1/4	0.089(4)	0.043(3)
O_{33}	8d	0.580(2)	0.667(1)	0.676(3)	0.043(3)
O_{34}	8d	0.933(2)	0.833(1)	0.665(3)	0.043(3)
O_{41}	4c	0.415(2)	1/4	0.575(3)	0.021(3)
O_{42}	4c	0.064(2)	1/4	0.585(3)	0.021(3)
O_{43}	8d	0.931(1)	0.585(1)	0.911(2)	0.021(3)
O_{44}	8d	0.581(1)	0.918(1)	0.935(2)	0.021(3)

Table 3
Atomic coordinates and isotropic displacement parameters for $Pb_3Mn_7O_{15}$ at 573 K.

Atom	Site	x	y	z	U_{iso} (Å^2)
Pb_1	6g	0.6124(1)	0.6124(1)	3/4	0.064(2)
Pb_2	6g	0.2642(1)	0.2642(1)	3/4	0.064(2)
Mn_1	12i	0.8311(2)	0.1689(2)	1/2	0.043(2)
Mn_2	8h	1/3	2/3	0.1474(2)	0.039(3)
Mn_3	6f	1/2	1/2	1/2	0.027(3)
Mn_4	2b	0	0	0	0.051(3)
O_1	24l	0.4918(7)	0.3288(9)	0.0806(5)	0.046(3)
O_2	12j	0.529(1)	0.179(1)	1/4	0.032(4)
O_3	12k	0.158(1)	0.158(1)	0.0791(6)	0.052(4)
O_4	12k	0.665(1)	0.665(1)	0.0730(8)	0.036(4)

Table 4
Atomic coordinates and isotropic displacement parameters for $Pb_3Mn_7O_{15}$ at 1073 K.

Atom	Site	x	y	z	U_{iso} (Å^2)
Pb_1	6g	0.6128(1)	0.6128(1)	3/4	0.096(1)
Pb_2	6g	0.26286(9)	0.26286(9)	3/4	0.095(1)
Mn_1	12i	0.8314(1)	0.1686(1)	1/2	0.056(2)
Mn_2	8h	1/3	2/3	0.1468(2)	0.059(2)
Mn_3	6f	1/2	1/2	1/2	0.044(2)
Mn_4	2b	0	0	0	0.065(4)
O_1	24l	0.4949(5)	0.3305(6)	0.0811(3)	0.056(2)
O_2	12j	0.5261(8)	0.1797(8)	1/4	0.044(3)
O_3	12k	0.1621(7)	0.1621(7)	0.0791(4)	0.070(3)
O_4	12k	0.6644(7)	0.6644(7)	0.0715(5)	0.048(3)

$Pb_3Mn_7O_{15}$ at 573 and 1073 K was refined using the structure of Zenzenite as an initial model. The results are listed in Tables 1, 3, and 4 and shown in Fig. 1b. In the numerical notation of atoms the first digit corresponds to the related sites in the orthorhombic and the hexagonal structures.

Fig. 3 demonstrates the temperature dependences of lattice parameter *a* obtained by us and the synchrotron XRD data [14]. The synchrotron data curve is smooth, whereas the curve obtained in a more thorough XRD (DRON-2) experiment on a single-crystal plate sample in narrower temperature range 130–250 K revealed two special features (Fig. 3) corresponding to the temperatures of possible phase transitions [12]. In addition, we measured the thermal expansion coefficient α in this temperature range. The temperature dependences of α along and across the plate are presented in Fig. 4a and b. The sharp peaks of the coefficient of thermal expansion (Fig. 4) are revealed at the temperatures different from features of the temperature dependences of lattice parameter ***a*** (Fig. 3). We still fail to explain this fact.

In our previous study [12] where we reported the calorimetric results, there was a pronounced magnetic lambda-peak at 140–150 K that we explained by the occurrence of the short-range order. Permittivity has anomalies in this temperature range [13]. This set of characteristics evidences that the occurrence of the short-range order is accompanied by their anomalous behavior correlating with the structural distortions.

We examined the effect of some technological parameters and synthesis conditions on the $Pb_3Mn_7O_{15}$ structure. No effects of crucible cooling rate, the lower limit of the furnace temperature down to which the temperature reduction program operates, mechanical drawing of the crystals, or washing them in a water solution of nitric acid on the structural characteristics of $Pb_3Mn_7O_{15}$ were found. We attempted to freeze the hexagonal high-temperature phase by rapid quenching of the sample at 1100 K. The PXRD of the sample taken prior to the thermal treatment appeared identical to that of the quenched sample.

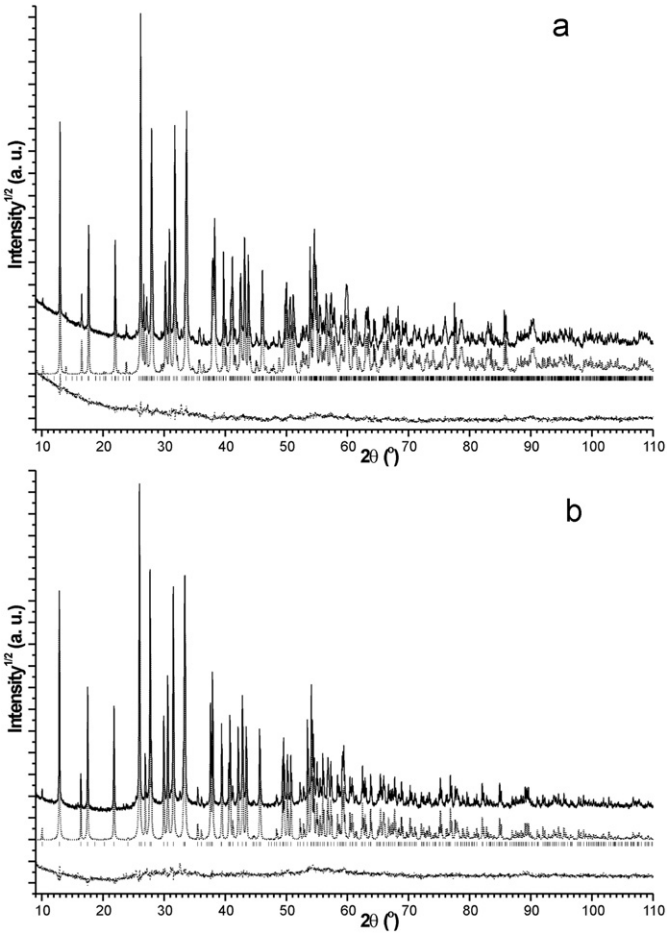

Fig. 1. Observed (solid line), calculated (dashed line) and difference (dots) PXRD patterns of $Pb_3Mn_7O_{15}$ at 298 K (a), and 1073 K (b) after the crystal structure refinement.

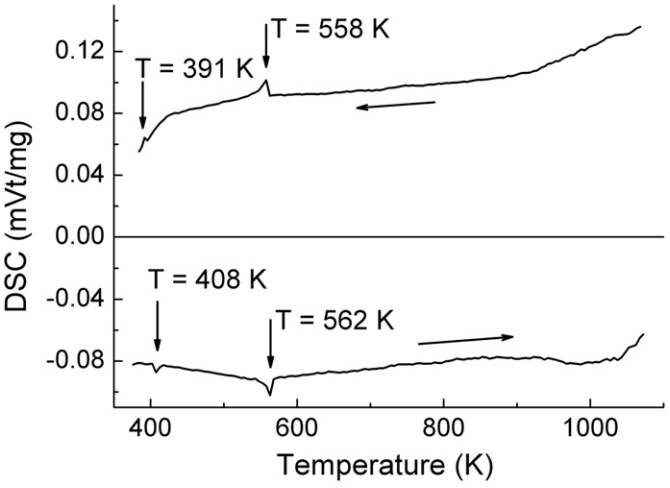

Fig. 2. DSC curves for heating and cooling cycles.

Exposure of the single crystals to nitric acid for three days had no effect on the structural properties of $Pb_3Mn_7O_{15}$ either.

4. Discussion

The XRD data on the observed high-temperature transition from the orthorhombic to the hexagonal phase were analyzed using the

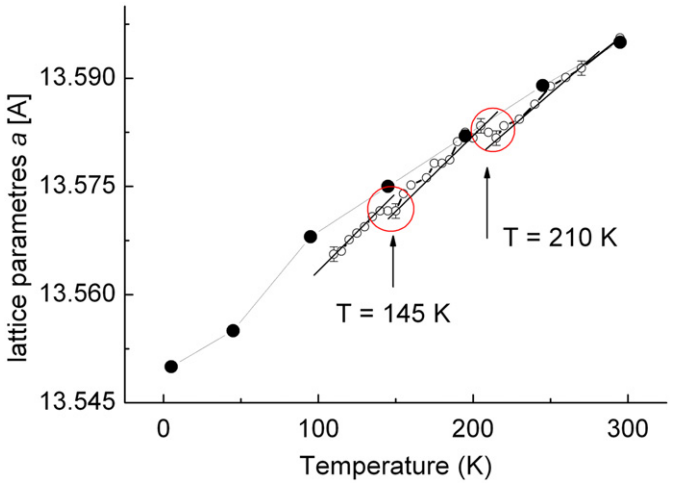

Fig. 3. Temperature dependence of lattice parameter a from laboratory XRD (open circles), and synchrotron [14] measurements (solid circles).

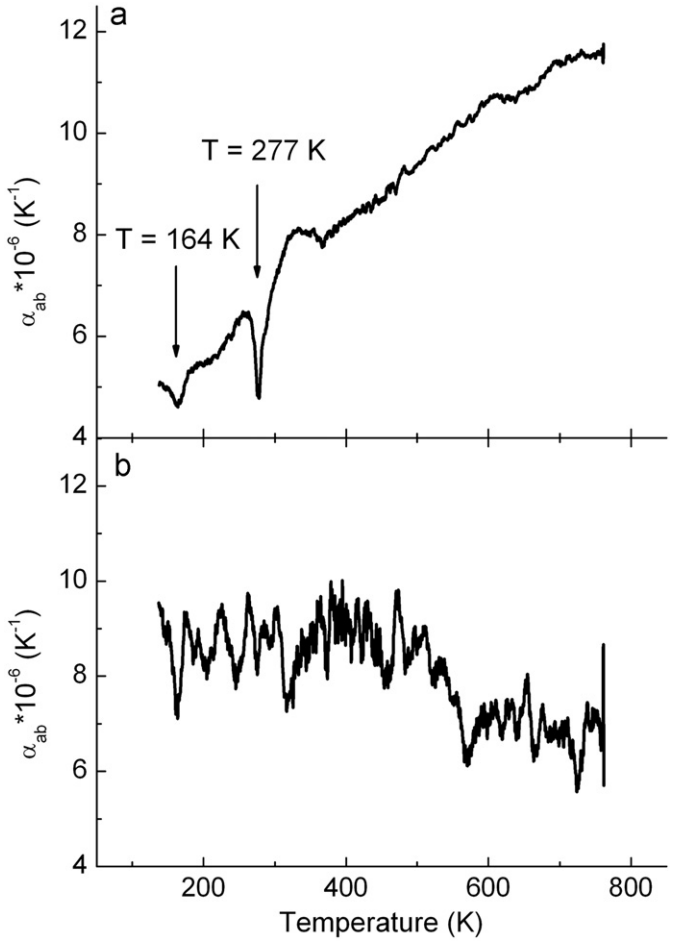

Fig. 4. Temperature dependence of thermal expansion coefficient α along (a), and across (b) the crystal.

group-theoretical methods [17,18]. The analysis allowed establishing general regularities of the structural changes and revealing the features of atom behavior during the phase transition.

According to the results reported in [19–23] and our examinations, the symmetry transition from $P6_3/mcm$ to Pnma can be described by one three-component phenomenological order parameter (OP) of the (η,0,0) type transformation by the irreducible representation (IR) M_2^- (1 2 −4) of the $P6_3/mcm$ group with k-vector of Brilluen zone (point M, k_{12}=(1/2,0,0)) (Fig. 5). Note that the critical IR M_2^- (1 2 −4) transforming the critical (η,0,0) OP satisfies the Landau and Lifshitz criteria [17] and makes it possible to transform the $P6_3/mcm$ phase to the Pnma phase by the second-order transition. In Fig. 6 the temperature dependence of hexagonal (pseudo-hexagonal before 405 K) lattice parameters a, b, and c at heating is shown. The jump on the c parameter curve at 405 K indicates that the transition is of the second order.

Thus, the symmetry transformation in the $Pb_3Mn_7O_{15}$ crystal can be schematically presented as $P6_3/mcm \xrightarrow[(\eta,0,0)]{M_2^-(12-4)}$ Pnma.

Cell parameters transform: $a_{ort}=c_{hex}$; $b_{ort}=2a_{hex}+b_{hex}$; $c_{ort}=b_{hex}$, where a_{ort}, b_{ort}, c_{ort} – basis vectors of cell of Pnma phase, a_{hex}, b_{hex}, c_{hex} – basis vectors of cell of $P6_3/mcm$ phase. The possible intermediate phases were identified using SUBGROUPGRAPH program [23] in Bilbao Crystallographic Server (Fig. 7).

Using the procedures of ISOTROPY [21] and ISODISPLACE [22] programs, we determined the noncritical IRs and OPs. The noncritical IRs are Γ_5^+ (1 6 − 1 1), Γ_1^+ (1 6 − 1), and M_1^+ (1 2 − 1).

For assignment of the atomic displacements and the critical and noncritical orderings, a composition of the mechanical and permutation representations was analyzed. The first is based on displacements of atoms of the structure; the second on a variation in populations of the positions occupied by atoms of the structure in the highly symmetric G_0 phase [18].

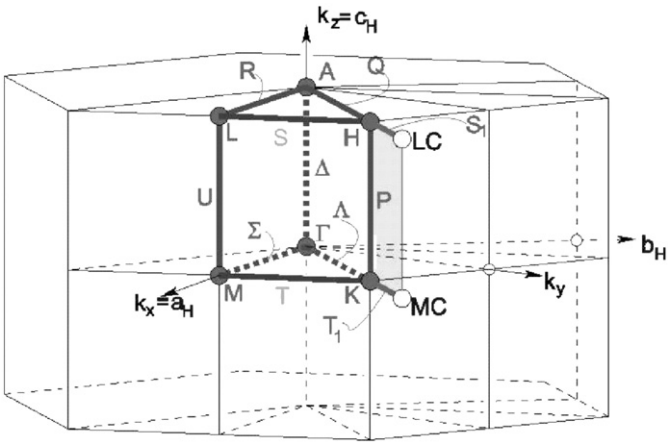

Fig. 5. Selected 1/6 part of the Brilluen zone for simple hexagonal lattice.

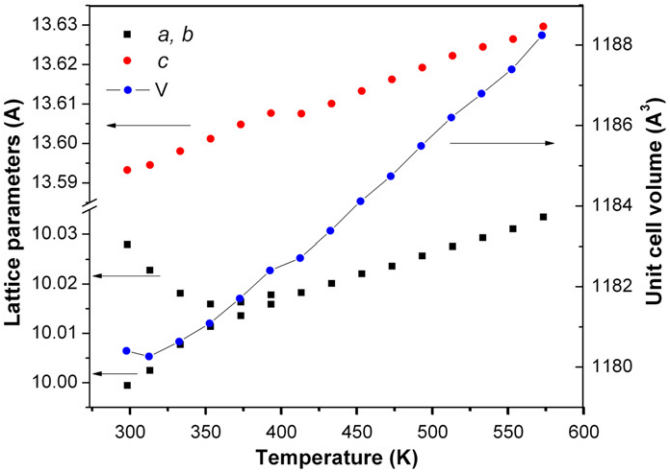

Fig. 6. Temperature dependence of hexagonal (pseudo-hexagonal before 405 K) lattice parameters a, b and c at heating.

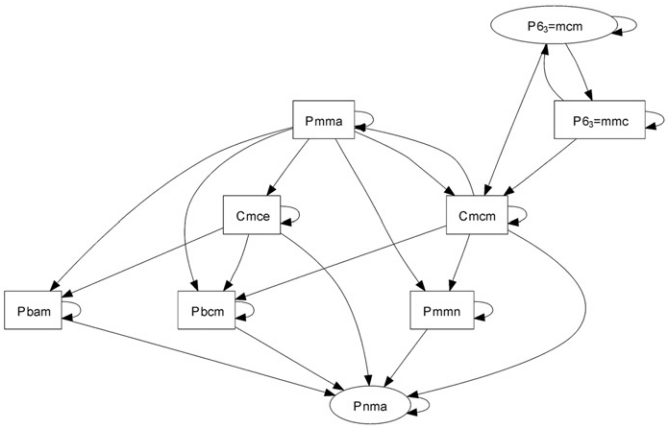

Fig. 7. The group–subgroup relation diagram for the transition between $P6_3/mcm$ and Pnma.

Thus, comparing positions of the atoms in the hexagonal and orthorhombic $Pb_3Mn_7O_{15}$ phases and expanding the displacements of atoms by the IRs of the G_0 group using the ISODISLACE program procedures [22], we established the critical and noncritical displacements. As one could expect, the maximal displacements of the atoms are related to the critical representation $M_2^-(1\,2\,-4)$. In particular, the maximal displacements described by this representation observed for a lead ion Pb_{21} (hereinafter the atoms are numbered according to Table 2) are $\Delta r(Pb_{21})=(-0.280$ Å, 0, 0.043 Å) in the reference frame coupled with the orthorhombic unit cell. It is seen that the displacement along the orthorhombic lattice axis a corresponding to the hexagonal lattice axis c is maximal. Other lead ions are displaced less by a factor of more than 2 as compared to the Pb_{21} displacements.

The remaining ions of the structure also undergo considerable, though less in their absolute magnitude, displacements related to this representation. For instance, the maximal displacements under the action of this representation observed for oxygen ions O_{11} and O_{12} are $\Delta r(O_{11})=(0.019$ Å, 0.067 Å, 0.190 Å) and $\Delta r(O_{12})=(-0.046$ Å, -0.050 Å, -0.222 Å) in the orthorhombic reference frame. The largest displacement among the manganese ions, $\Delta r(Mn_{31})=(-0.175$ Å, 0, 0.09 Å), is observed for Mn_{31}. As in the case of the lead ion Pb_{21}, the Mn_{31} displacement occurs mainly along the orthorhombic axis *a*.

The most noticeable of the mentioned noncritical displacements are those related to the noncritical IR $\Gamma_5^+(1\,6\,-1\,1)$. However, all the noncritical displacements are considerably smaller than the critical ones. In particular, the longest displacement related to $\Gamma_5^+(1\,6\,-1\,1)$ is observed for Pb_{22} at the vector $\Delta r(Pb_{22})=(-0.100$ Å, 0.013 Å, -0.065 Å), which is several times shorter than the critical Pb_{21} displacements.

As it is seen from the structural data (Tables 2–4), the atomic ordering may play an appreciable role in the phase transition. Meanwhile, judging from the entropy value (Fig. 2), the phase transition in $Pb_3Mn_7O_{15}$ is related rather to the atom displacements [24] than to the ordering process. To complete the picture of possible variations in the structure of the hexagonal $Pb_3Mn_7O_{15}$ phase, we analyzed the permutation representation using the procedures of the ISODISPLACE program [22]. For the sake of simplicity, we took only heavy ion positions.

The permutation representation at the positions occupied by Pb and Mn_4 ions does not include the $M_2^-(1\,2\,-4)$ representation, which implies that no ordering of these ions can occur during the phase transition.

5. Conclusion

Having analyzed the results obtained, we concluded that the $Pb_3Mn_7O_{15}$ crystals undergo a phase transition from the orthorhombic Pnma to the hexagonal $P6_3/mcm$ structure. The combined investigations revealed a series of other jumps of the material properties in the temperature range 4.2–1100 K detected by the XRD, calorimetric, magnetic, and DSC measurements. All the detected effects correlate with one another.

Using the group-theoretical methods, we showed that the symmetry transformation in phase transition can be outlined as $P6_3/mcm \xrightarrow[(\eta,0,0)]{M_2^-(12-4)}$ Pnma. The symmetry analysis suggests that the phase transition is related to the critical (η, 0, 0) RR transformation by the critical representation M_2^-. A critical ion of the phase transition is the Pb_{21} ion having the maximal displacement. Judging by the specific heat variation during the phase transition, the ordering process is found to be less probable.

Acknowledgments

This study was supported by the Russian Foundation for Basic Research 'Siberia', Project no. 09-02-98003, and the Siberian Branch of the Russian Academy of Sciences, integration Project no. 101. This work was partially supported by the Russian Ministry of Education and Science Federal Program Grant P2430.

References

[1] P.B. Darriet, M. Devalette, B. Latourrette, Acta Cryst. B 34 (1978) 3528.
[2] R.E. Marsh, F.H. Herbstein, Acta Cryst. B 39 (1983) 280.
[3] Y. Le Page, L.D. Calvert, Acta Cryst. C 40 (1984) 1787.
[4] D. Holtstam, B. Lindqvist, M. Johnsson, R. Norrestam, Can. Mineral. 29 (1991) 347.
[5] N. Henry, L. Burylo-Dhuime, F. Abraham, O. Mentre, Phys. Inorg. Chem. 4 (2002) 1023.
[6] K. Wakiya, H. Sato, A. Miyazaki, T. Enoki, M. Isobe, Y. Ueda, J. Alloys Compd. 317-318 (2001) 115.
[7] Artem M. Abakumov, Joke Hadermann, Alexander A. Tsirlin, Haiyan Tan, Jo Verbeeck, Haitao Zhang, Evgeny V. Dikarev, Roman V. Shpanchenko, Evgeny V. Antipov, J. Solid State Chem. 182 (2009) 2231.
[8] Toshiaki Hirohiko Sato, Jun-Ichi Enoki, Yamaura, Naoichi Yamamoto, Phys. Rev. B. 59 (1999) 12836.
[9] Toshiaki Hirohiko Sato, Masahiko Enoki, Isobe, Yutaka Ueda, Phys. Rev. B 61 (2000) 3563.
[10] Ram Seshadri, Guido Baldinozzi, Claudia Felser, Wolfgang Tremel, J. Mater. Chem. 9 (1999) 2463.
[11] N.V. Volkov, K.A. Sablina, O.A. Bayukov, E.V. Eremin, G.A. Petrakovskii, D.A. Velikanov, A.D. Balaev, A.F. Bovina, P. Böni, E. Clementyev, J. Phys. Condens. Matter 20 (2008) 055217.
[12] N.V. Volkov, K.A. Sablina, E.V. Eremin, P. Böni, V.R. Shah, I.N. Flerov, A. Kartashev, J.C.E. Rasch, M. Boehm, J. Schefer, J. Phys. Condens. Matter 20 (2008) 445217.
[13] N.V. Volkov, E.V. Eremin, K.A. Sablina, N.V. Sapronova, J. Phys. Condens. Matter 22 (2010) 375901.
[14] Julia C.E. Rasch, D.V. Sheptyakov, J. Schefer, L. Keller, M. Boehm, F. Gozzo, N.V. Volkov, K.A. Sablina, G.A. Petrakovskii, H. Grimmer, K. Conder, J.F. Loffler, J. Solid State Chem. 182 (2009) 1188.
[15] H.M. Rietveld, J. Appl. Cryst. 2 (1969) 65.
[16] L.A. Solovyov, J. Appl. Cryst. 37 (2004) 743.
[17] Yu.A. Izyumov, V.N. Syromyatnikov, Phase Transitions and Crystal Symmetry, Nauka, Moscow, 1984.
[18] V.P. Sakhnenko, V.M. Talanov, G.M. Chechin, Fiz. Met. Metalloved. 62 (1986) 847.
[19] J.M. Perez-Mato, J.L. Manes, M.J. Tello, F.J. Zuniga, J. Phys. C: Solid State Phys. 14 (1981) 1121.
[20] Yu.M. Gufan, V.P. Dmitriev, S.B. Roshal', V.I. Snezhkov, Izd. Rostov. Univ. (1990) 256.
[21] H.T. Stokes, D.M. Hatch, B.J. Campbell, Isotropy, 2007stokes.byu.edu/isotropy.html.
[22] B.J. Campbell, H.T. Stokes, D.E. Tanner, D.M. Hatch, J. Appl. Crystallogr. 39 (2006) 607.
[23] S. Ivantchev, E. Kroumova, M.I. Aroyo, J.M. Perez-Mato, J.M. Igartua, G. Madariaga, H. Wondratschek, J. Appl. Cryst. 35 (2002) 511.
[24] I.N. Flerov, M.V. Gorev, K.S. Aleksandrov, A. Tressaud, J. Grannec, M. Couzi, Mater. Sci. Eng. R24 (1998) 81.